

**Confinement catalysis of the single atomic vacancy assisted with aliovalent ion doping
enabled efficient NO electroreduction to NH₃**

Bingling He^{1,3}, Peng Lv^{1,3}, Donghai Wu^{1,3}, Xue Li^{1,3}, Rui Zhu^{1,3}, Ke Chu⁴, Dongwei Ma^{1,3*} and
Yu Jia^{1,2,3*}

¹*Key Laboratory for Special Functional Materials of Ministry of Education, and School of
Materials Science and Engineering, Henan University, Kaifeng 475004, China*

²*International Laboratory for Quantum Functional Materials of Henan, and School
of Physics, Zhengzhou University, Zhengzhou 450001, China*

³*Joint Center for Theoretical Physics, and Center for Topological Functional Materials, Henan
University, Kaifeng 475004, China*

⁴*School of Materials Science and Engineering, Lanzhou Jiaotong University, Lanzhou 730070,
China*

Supporting Information

* Corresponding author. E-mail: madw@henu.edu.cn (Dongwei Ma)

* Corresponding author. E-mail: jiayu@henu.edu.cn (Yu Jia)

Table S1 Zero-point energy corrections and entropic contributions (at 298.15 K) to the free energies.

species	ΔE_{ZPE} (eV)	$T\Delta S$ (eV)
H ₂ O	0.56	0.67
H ₂	0.27	0.40
NO	0.12	0.65
NH ₃	0.89	0.60
*H	0.19	0.01
*NO	0.20	0.10
*NOH	0.46	0.10
*N	0.10	0.02
*NH	0.42	0.03
*NH ₂	0.74	0.05
*NH ₃	1.03	0.11
*N+*NO	0.27	0.17

Table S2 The potential-determining steps (PDS) and limiting potential (U_L) for NORR on TM@MoS_v.

TM@MoS _v	PDS	U_L (V)
Sc	$*\text{NH}_2 + \text{H}^+ + \text{e}^- \rightarrow *\text{NH}_3$	-0.70
Ti	$*\text{NH}_2 + \text{H}^+ + \text{e}^- \rightarrow *\text{NH}_3$	-0.60
V	$*\text{NH}_2 + \text{H}^+ + \text{e}^- \rightarrow *\text{NH}_3$	-1.03
Cr	$*\text{NH}_2 + \text{H}^+ + \text{e}^- \rightarrow *\text{NH}_3$	-0.83
Mn	$*\text{NH}_2 + \text{H}^+ + \text{e}^- \rightarrow *\text{NH}_3$	-0.61
Fe	$*\text{NH}_2 + \text{H}^+ + \text{e}^- \rightarrow *\text{NH}_3$	-0.58
Co	$*\text{NH}_2 + \text{H}^+ + \text{e}^- \rightarrow *\text{NH}_3$	-0.55
Ni	$*\text{NH}_2 + \text{H}^+ + \text{e}^- \rightarrow *\text{NH}_3$	-0.39
Cu	$*\text{NH}_2 + \text{H}^+ + \text{e}^- \rightarrow *\text{NH}_3$	-0.41
Y	$*\text{NH}_2 + \text{H}^+ + \text{e}^- \rightarrow *\text{NH}_3$	-0.75
Zr	$*\text{NH}_2 + \text{H}^+ + \text{e}^- \rightarrow *\text{NH}_3$	0.68
Nb	$*\text{NH}_2 + \text{H}^+ + \text{e}^- \rightarrow *\text{NH}_3$	-1.18
Mo	$*\text{NH} + \text{H}^+ + \text{e}^- \rightarrow *\text{NH}_2$	-1.55
Tc	$*\text{NH}_2 + \text{H}^+ + \text{e}^- \rightarrow *\text{NH}_3$	-0.60
Ru	$*\text{NH}_2 + \text{H}^+ + \text{e}^- \rightarrow *\text{NH}_3$	-0.37
Rh	$*\text{NH}_2 + \text{H}^+ + \text{e}^- \rightarrow *\text{NH}_3$	-0.67
Pd	$*\text{NH}_2 + \text{H}^+ + \text{e}^- \rightarrow *\text{NH}_3$	-0.45
Ag	$*\text{NH}_2 + \text{H}^+ + \text{e}^- \rightarrow *\text{NH}_3$	-0.48
La	$*\text{NH} + \text{H}^+ + \text{e}^- \rightarrow *\text{NH}_2$	-0.15
Hf	$*\text{NH}_2 + \text{H}^+ + \text{e}^- \rightarrow *\text{NH}_3$	-0.71
Ta	$*\text{NH}_2 + \text{H}^+ + \text{e}^- \rightarrow *\text{NH}_3$	-1.20
W	$*\text{NH} + \text{H}^+ + \text{e}^- \rightarrow *\text{NH}_2$	-1.59
Re	$*\text{NH} + \text{H}^+ + \text{e}^- \rightarrow *\text{NH}_2$	-0.58
Os	$*\text{NH}_2 + \text{H}^+ + \text{e}^- \rightarrow *\text{NH}_3$	-0.26
Ir	$*\text{NH}_2 + \text{H}^+ + \text{e}^- \rightarrow *\text{NH}_3$	-0.74
Pt	$*\text{NH}_2 + \text{H}^+ + \text{e}^- \rightarrow *\text{NH}_3$	-0.46
Au	$*\text{NH}_2 + \text{H}^+ + \text{e}^- \rightarrow *\text{NH}_3$	-0.49

Table S3 The potential-determining steps (PDS) and limiting potential (U_L) for NORR in literatures.

Systems	PDS	U_L (V)
MnO _{2-x} (211)	*NOH+H ⁺ +e ⁻ →*N+H ₂ O	-0.27 ¹
Zr-C ₂ N	*NO+H ⁺ +e ⁻ →*HNO	-0.29 ²
MoS ₂ (101)	*NH ₂ +H ⁺ +e ⁻ →*NH ₃	-0.30 ³
NiO (200)	*NO+H ⁺ +e ⁻ →*HNO	-0.14 ⁴
Bi (012)	*NO+H ⁺ +e ⁻ →*NOH	-0.66 ⁵
FeP (202)	*NH ₂ +H ⁺ +e ⁻ →*NH ₃	-0.22 ⁶
Ru-LCN	*NO+H ⁺ +e ⁻ →*HNO	-0.27 ⁷
Cr ₂ -C ₂ N	*NO+H ⁺ +e ⁻ →*HNO	-0.05 ⁸
Co-N ₄ /graphene	*NO+H ⁺ +e ⁻ →*HNO	-0.12 ⁹
Cu@g-C ₃ N ₄	*NO+H ⁺ +e ⁻ →*HNO	-0.37 ¹⁰
Cu@h-BN	*NO+H ⁺ +e ⁻ →*HNO	-0.23 ¹¹
Nb ₂ B ₂	*NO+H ⁺ +e ⁻ →*NOH	-0.11 ¹²
Hf ₂ B ₂	*NO+H ⁺ +e ⁻ →*NOH	-0.17 ¹²
Pt (111)	*NO+H ⁺ +e ⁻ →*NOH	-0.28 ¹³
Pt (100)	*NO+H ⁺ +e ⁻ →*HNO	-0.32 ¹³
Ni ₂ P (111)	*NO+H ⁺ +e ⁻ →*NOH	-0.61 ¹⁴

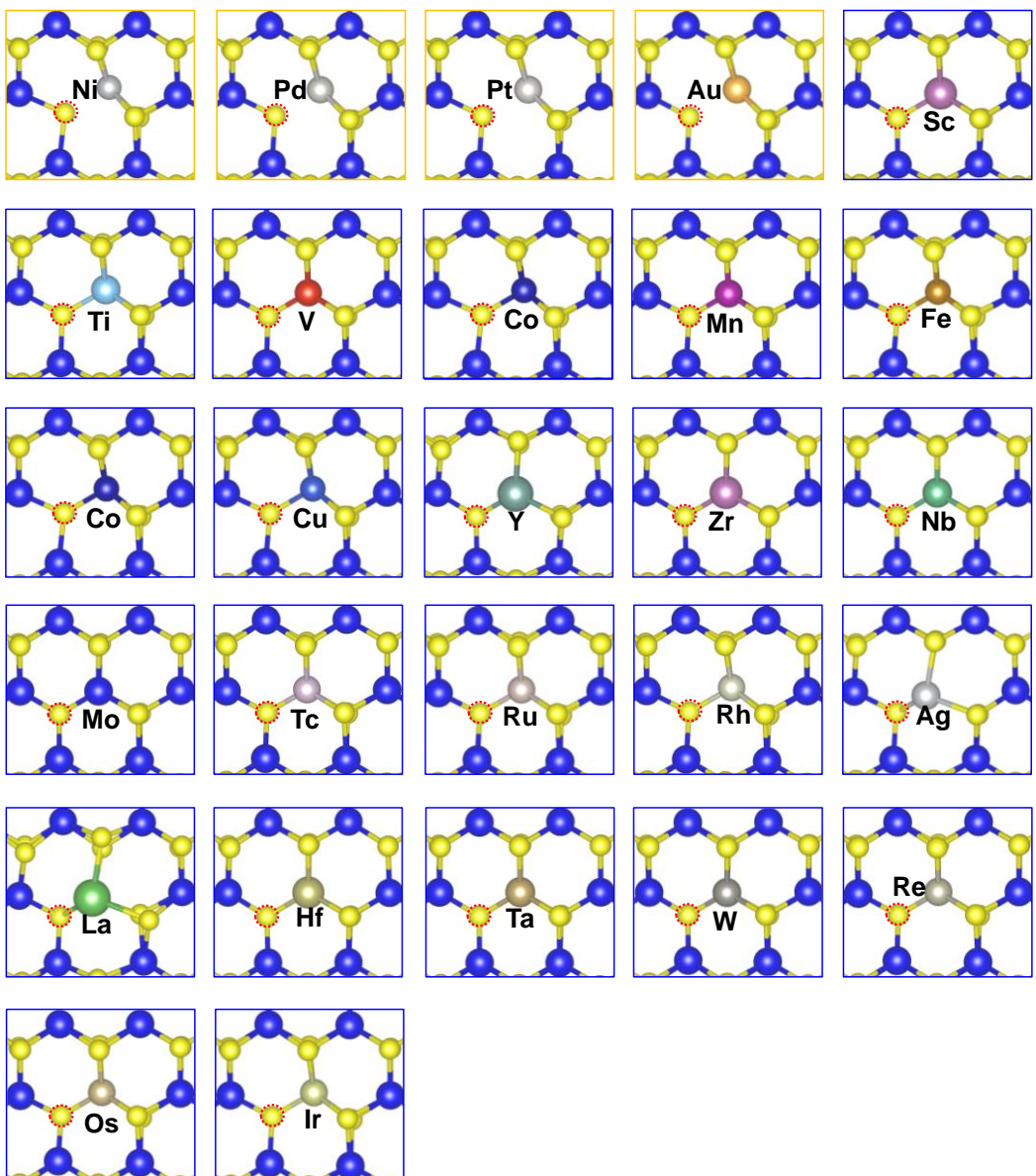


Fig. S1 The local atomic structures of various TM@MoS_v. The pictures with the ginger border represent the asymmetric local configurations of TM@MoS₂, while the others are the symmetric ones. The red dashed circle indicates the rough position of the S SAV.

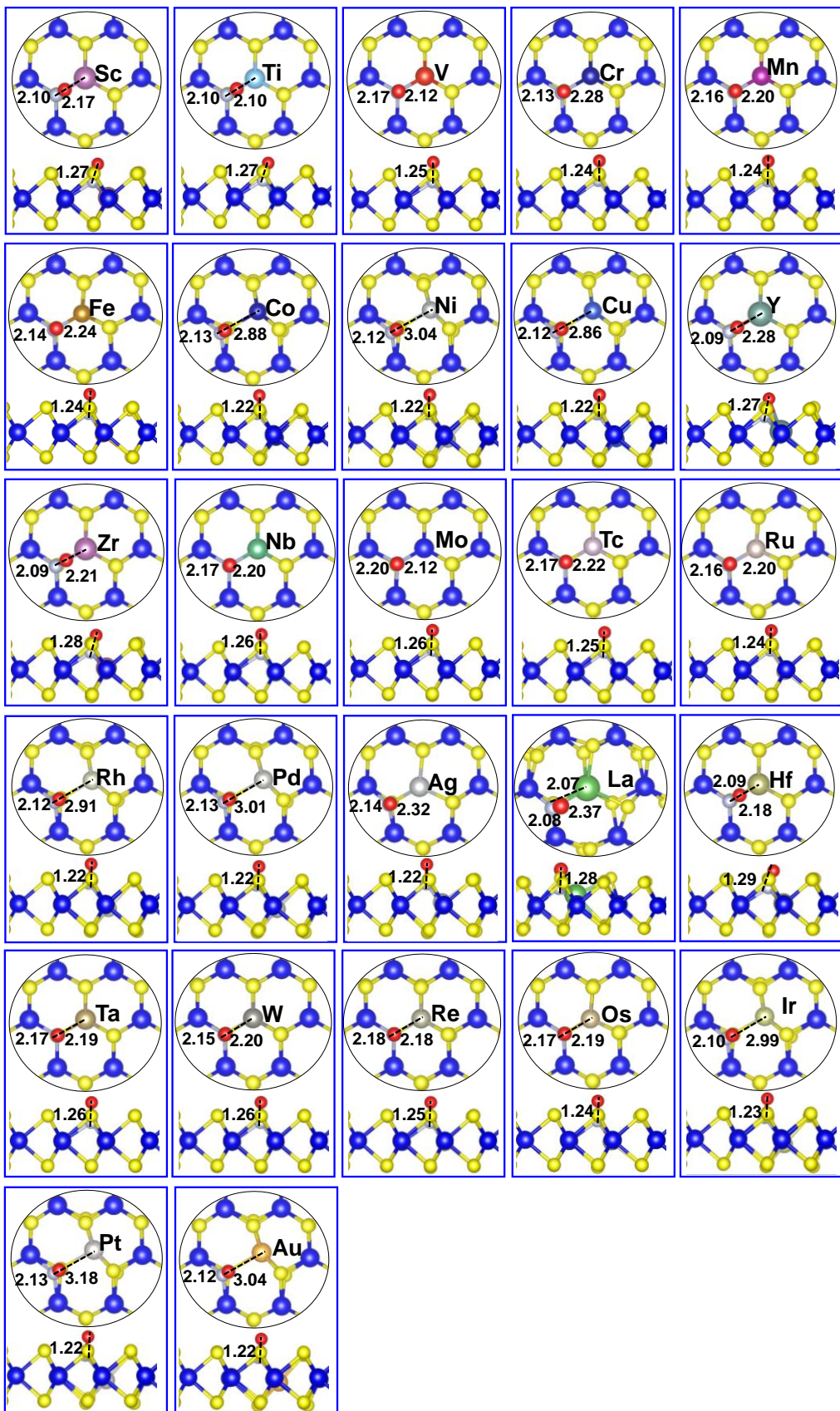


Fig. S2 Local atomic structures of NO-adsorbed TM@ MoS_v . The key bond lengths are given.

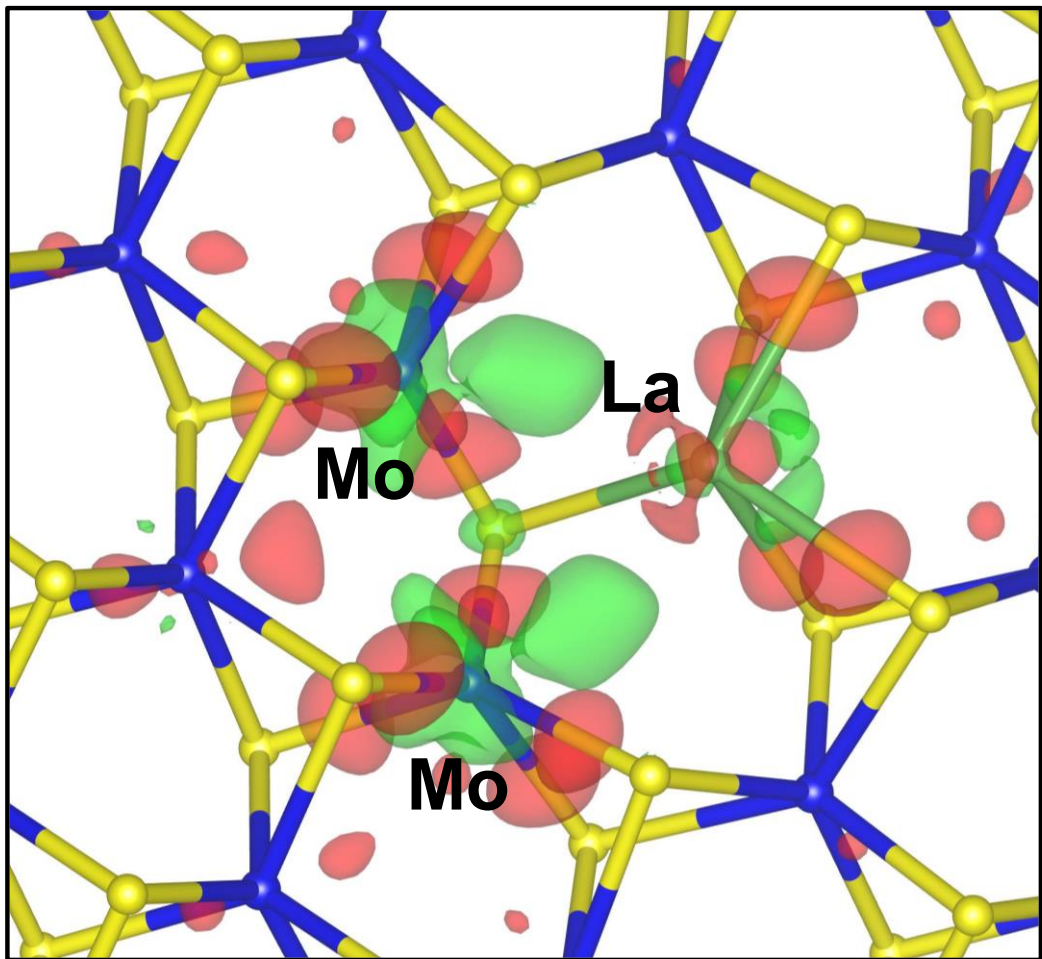


Fig. S3 The charge density difference (CDD) for two Mo and one La doping in MoS₂. The green and red regions denote the electron accumulation and depletion, respectively, and the isosurface value is set to be 0.01 e/bohr³.

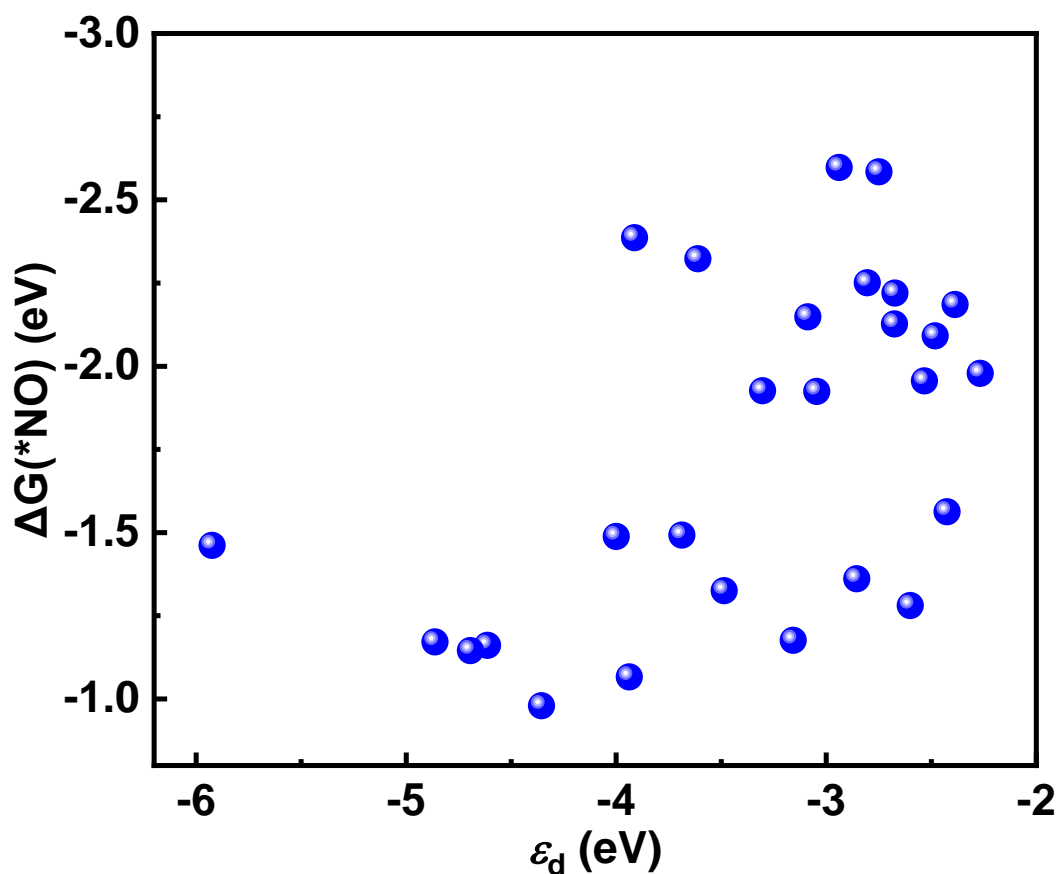
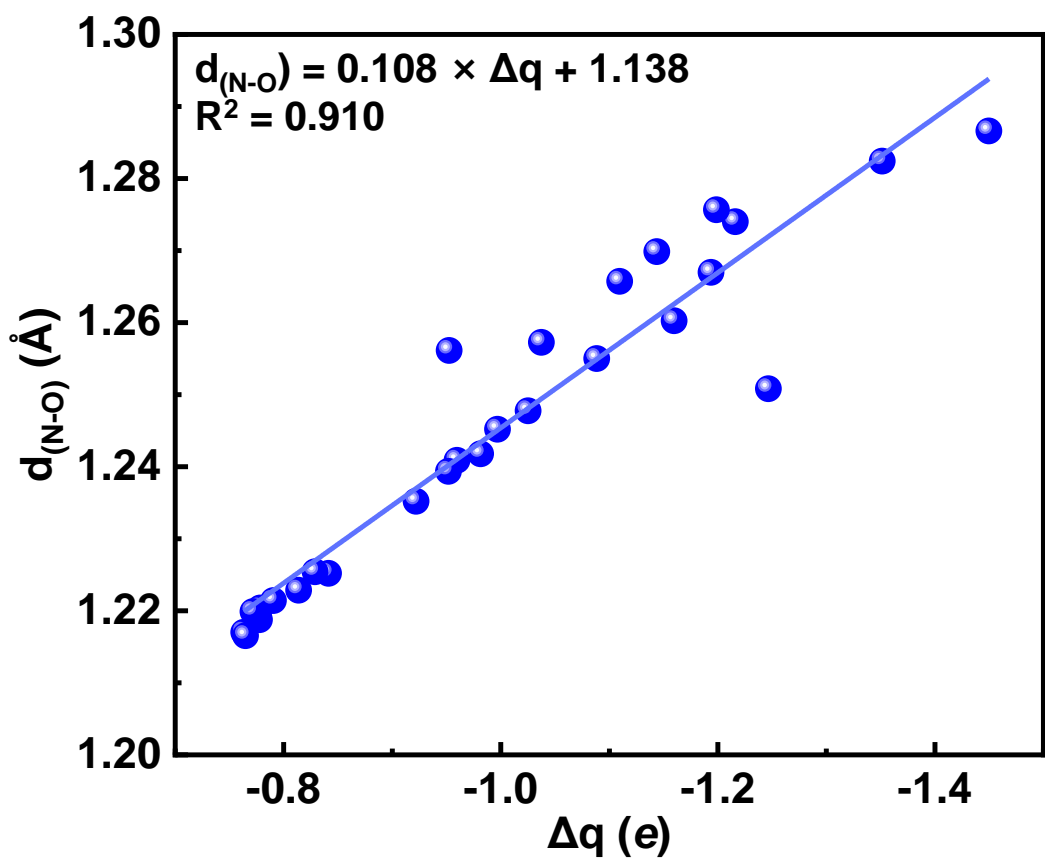
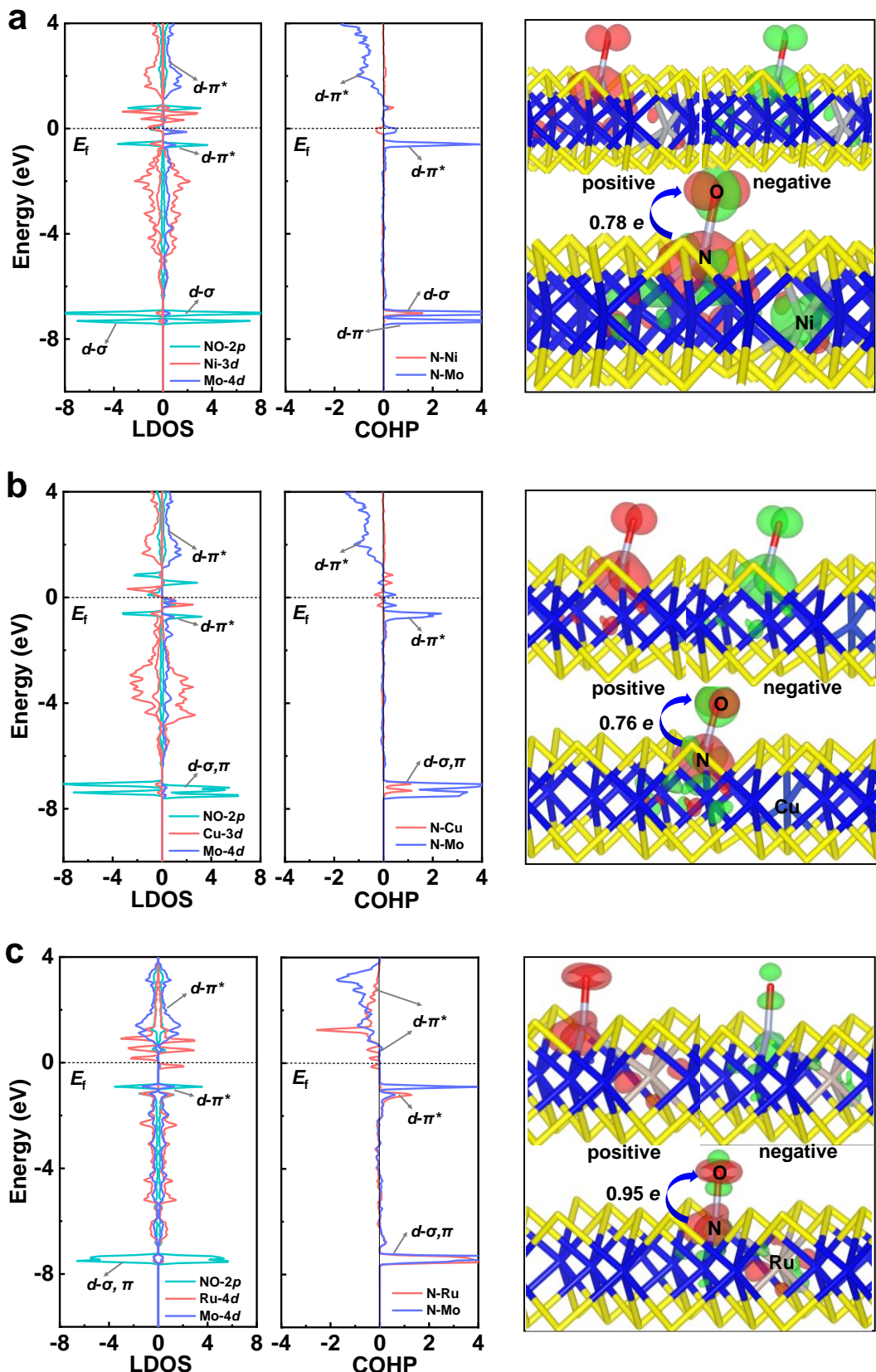
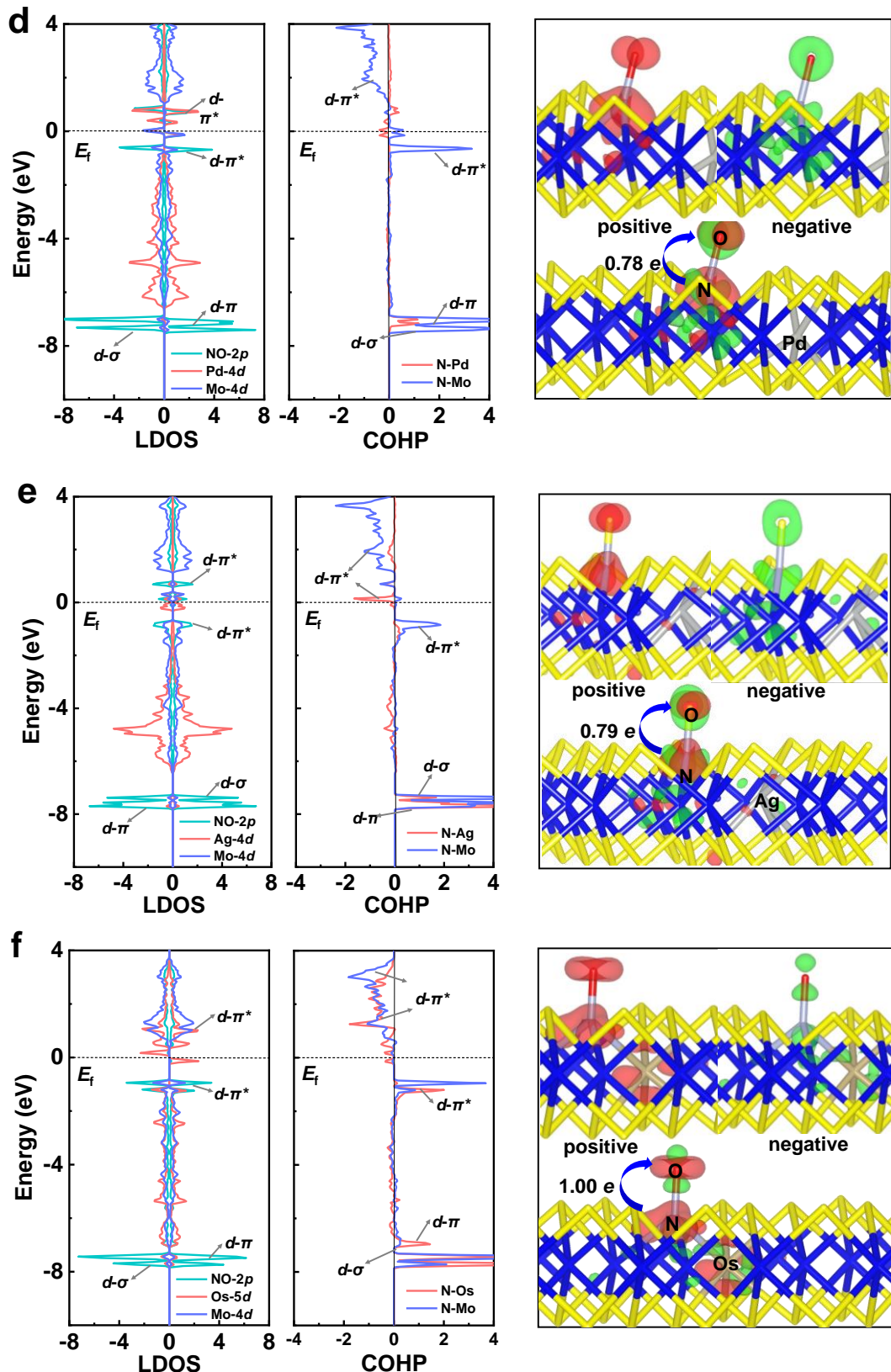


Fig. S4 The binding free energy of NO ($\Delta G(^*\text{NO})$) on TM@MoS_v versus the corresponding d-band center (ε_d) of TM.







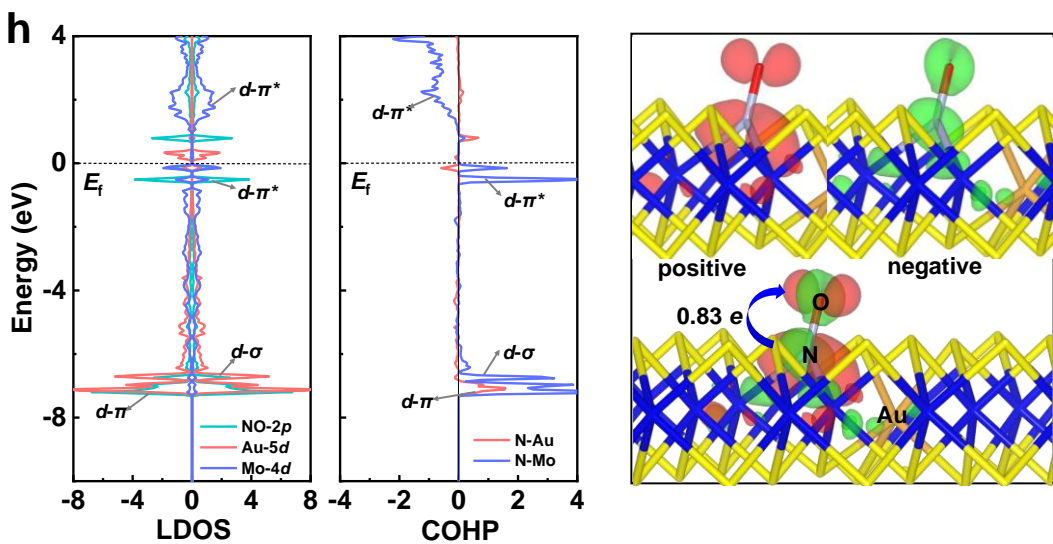
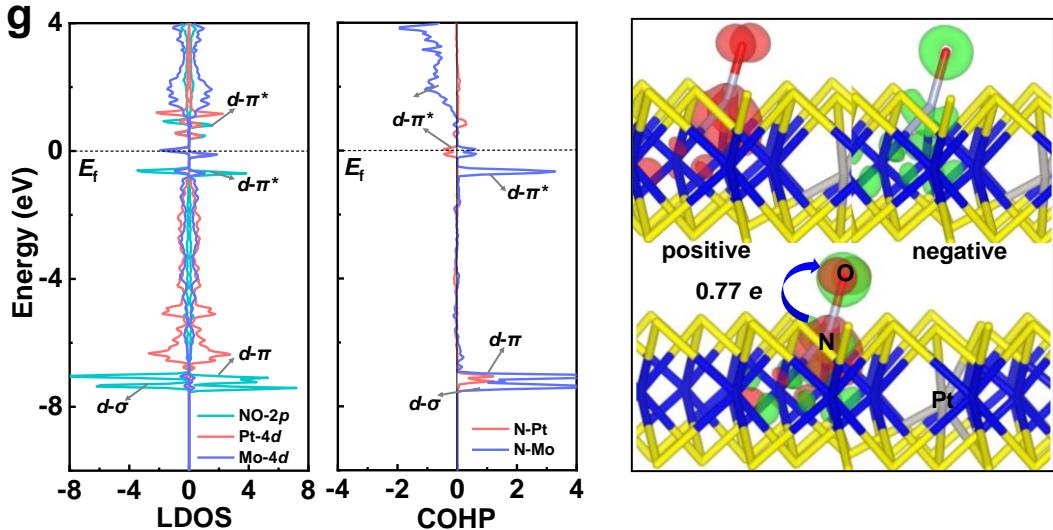


Fig. S6 The LDOS, COHP and CDD for NO adsorption on (a) Ni@MoS_v, (b) Cu@MoS_v, (c) Ru@MoS_v, (d) Pd@MoS_v, (e) Ag@MoS_v, (f) Os@MoS_v, (g) Pt@MoS_v, and (h) Au@MoS_v. In LDOS and COHP, the Fermi level (E_f) is set to 0 eV. In CDD for NO adsorption on various TM@MoS_v, the green and red regions denote the electron accumulation and depletion, respectively, and the isosurface value is set to be 0.01 e/bohr³.

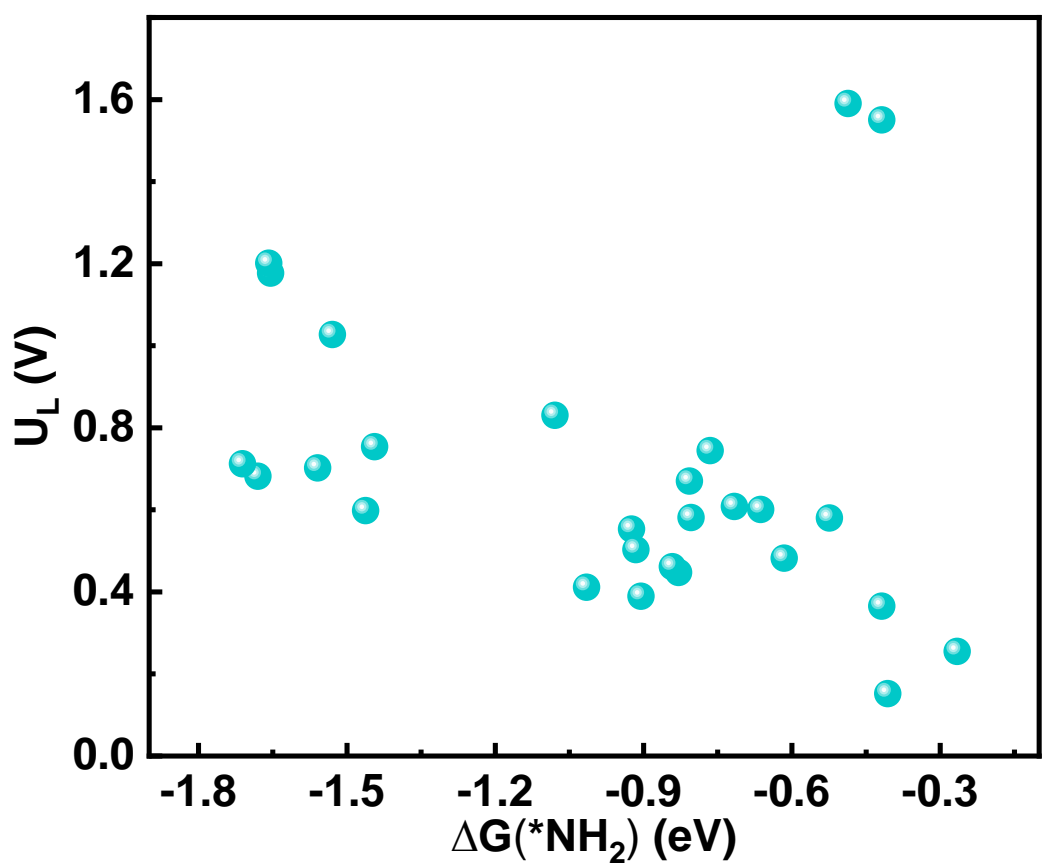
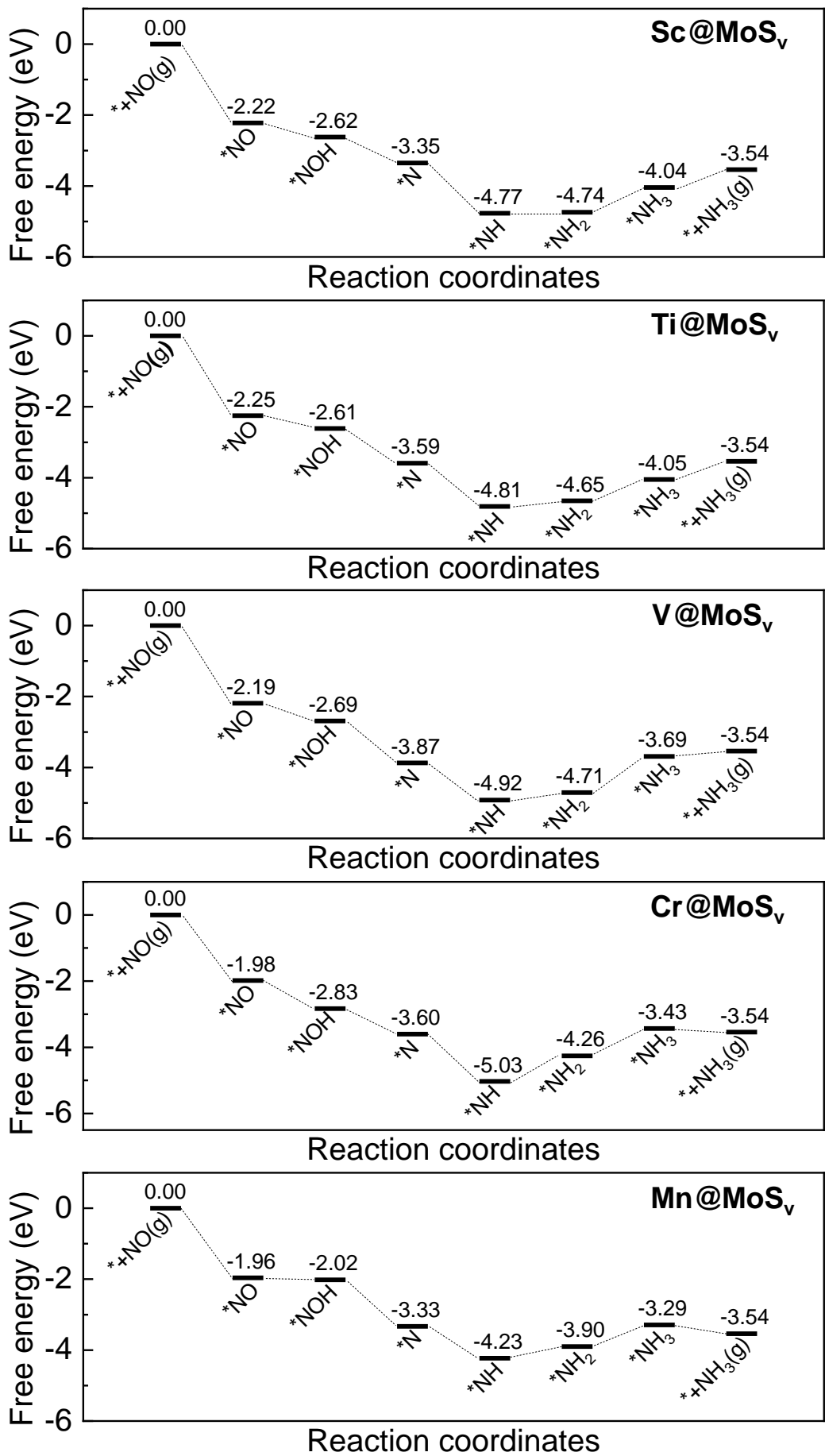
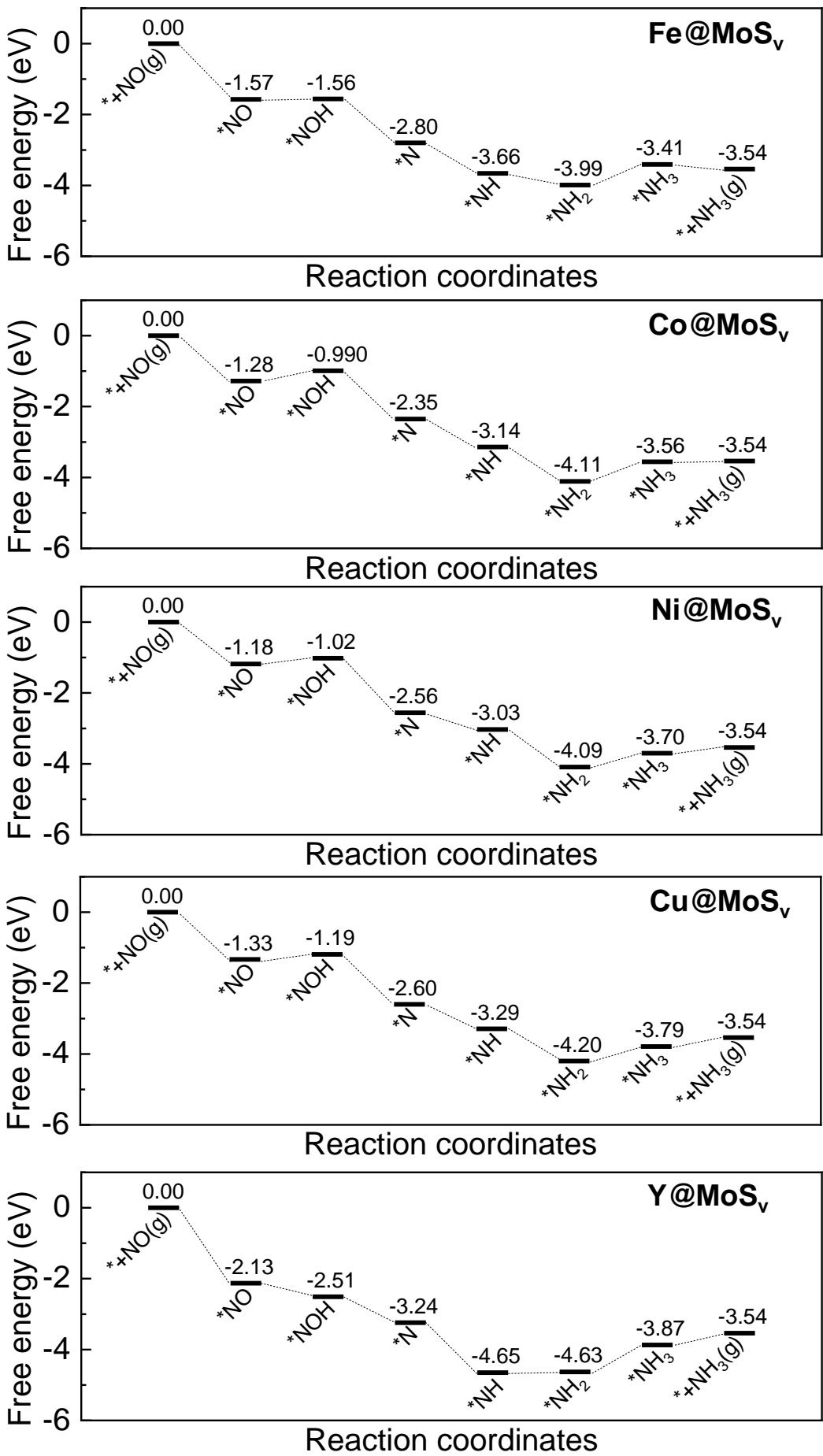
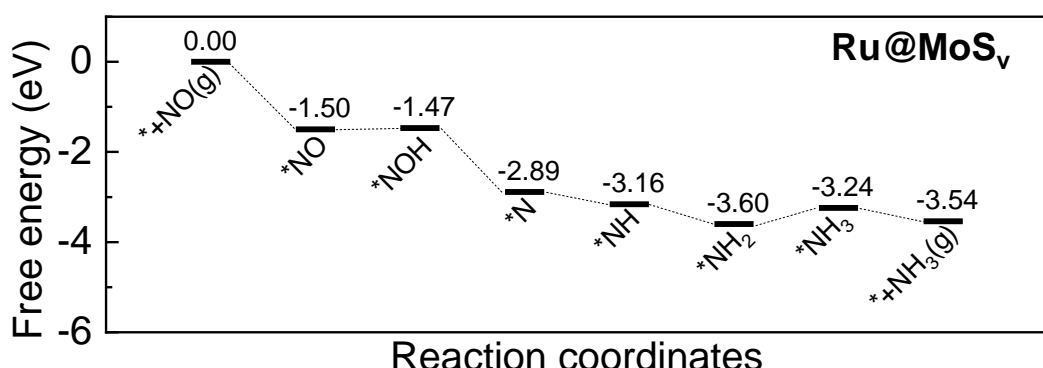
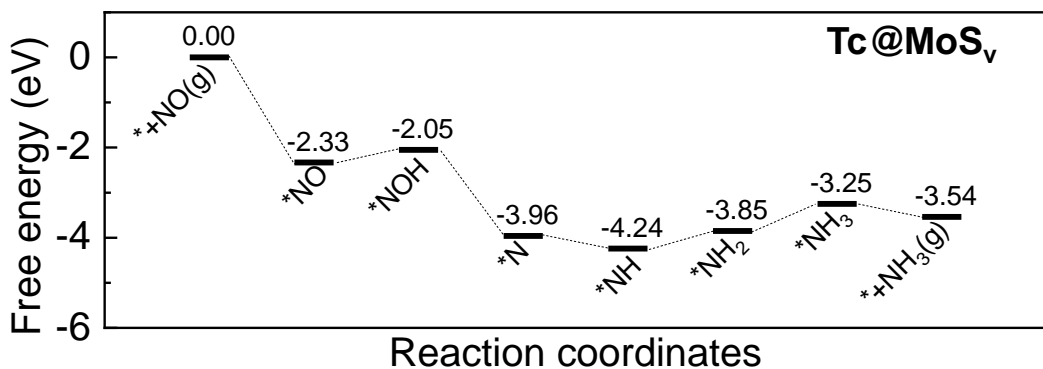
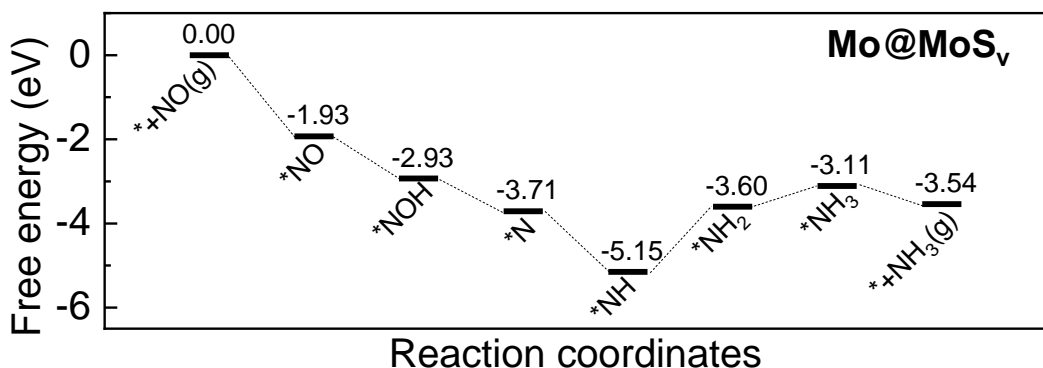
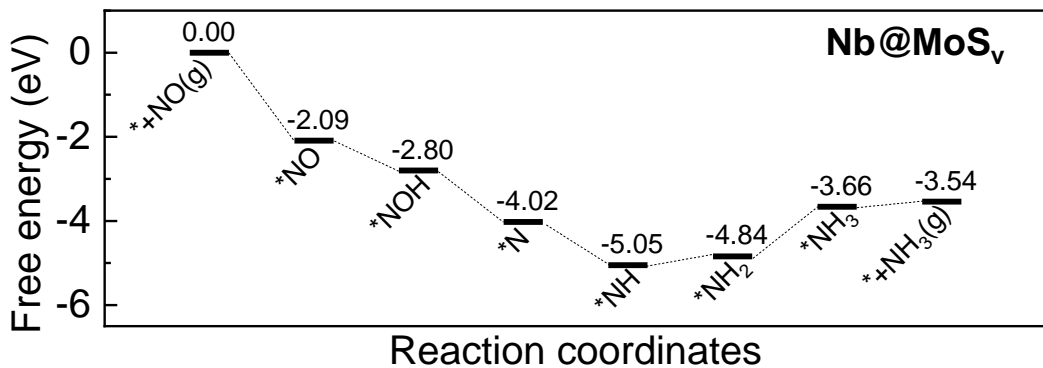
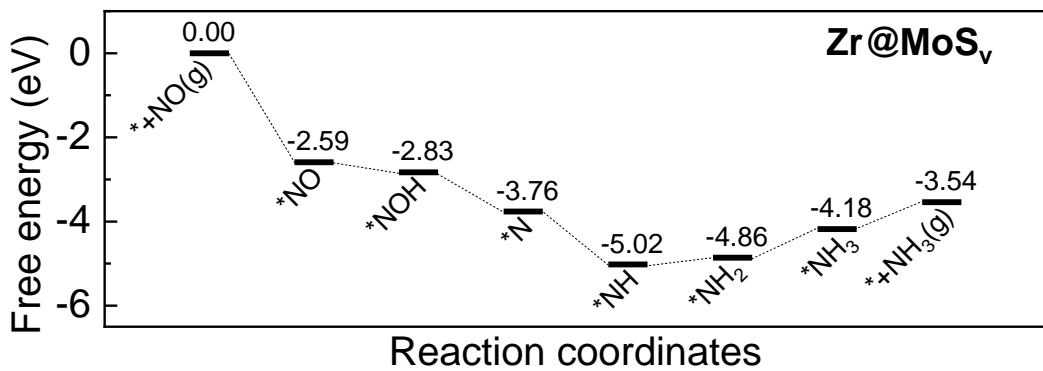
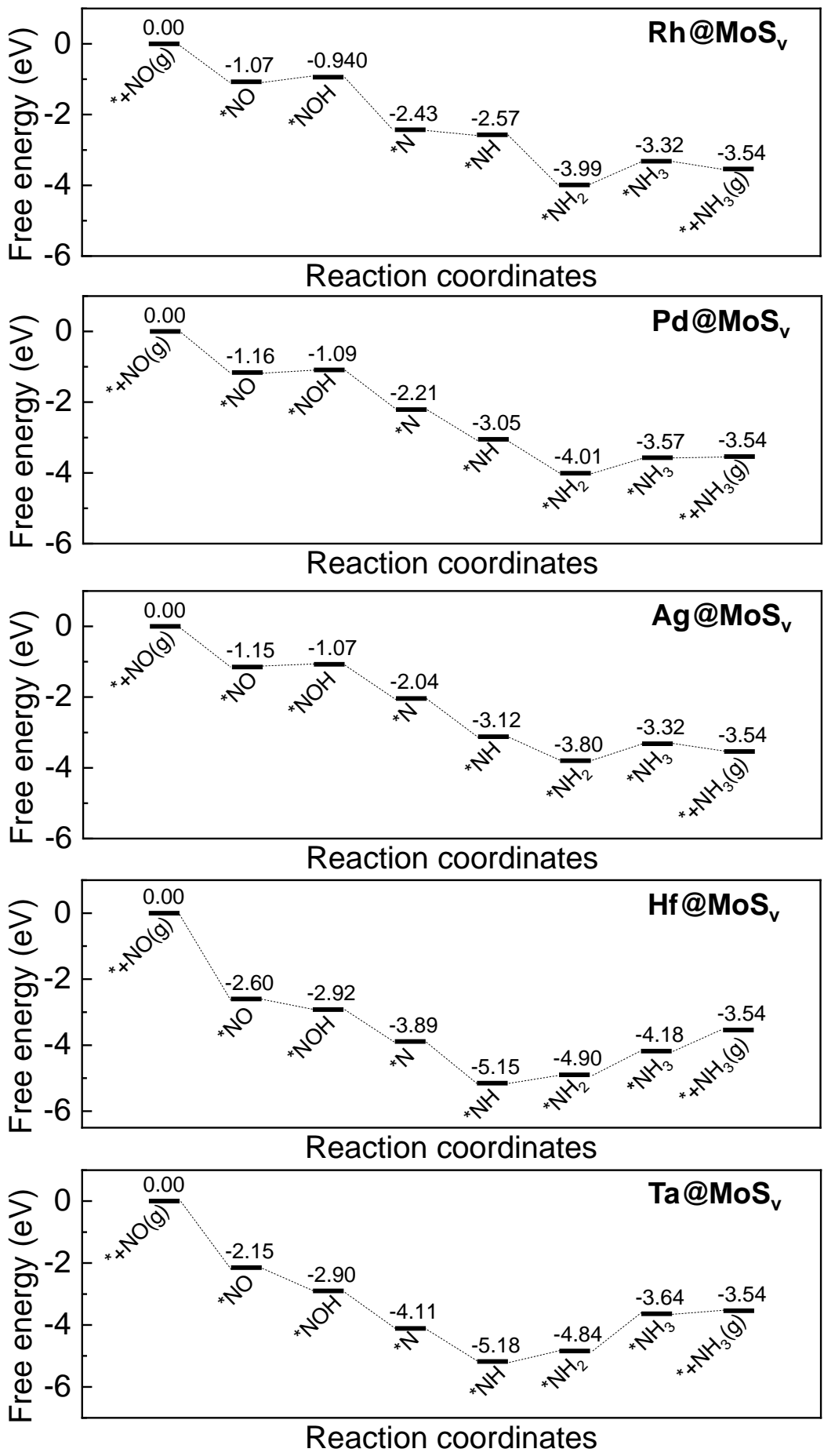


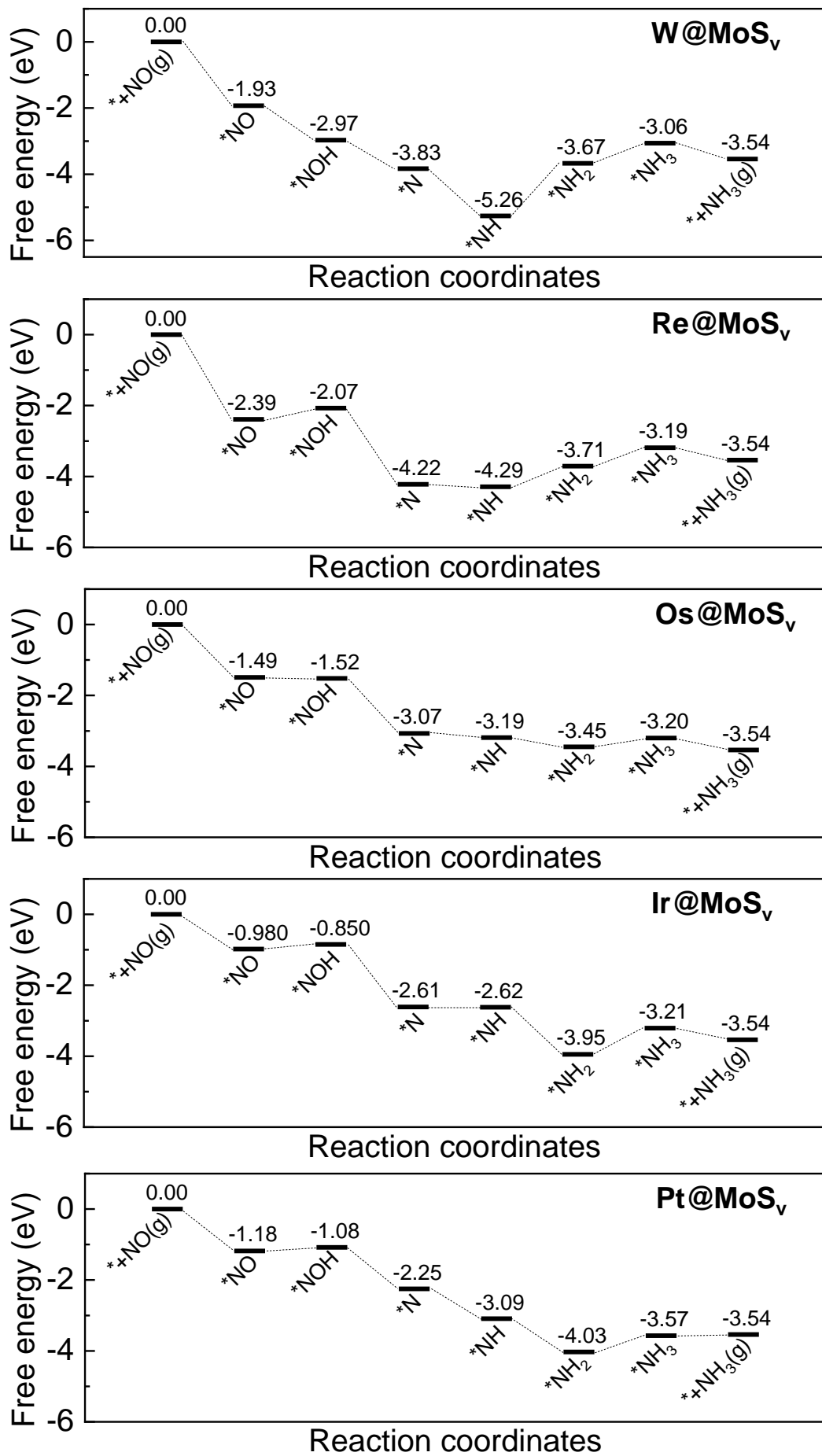
Fig. S7 The NORR limiting potential (U_L) versus the corresponding NH_2 binding free energy ($\Delta G(^*\text{NH}_2)$).











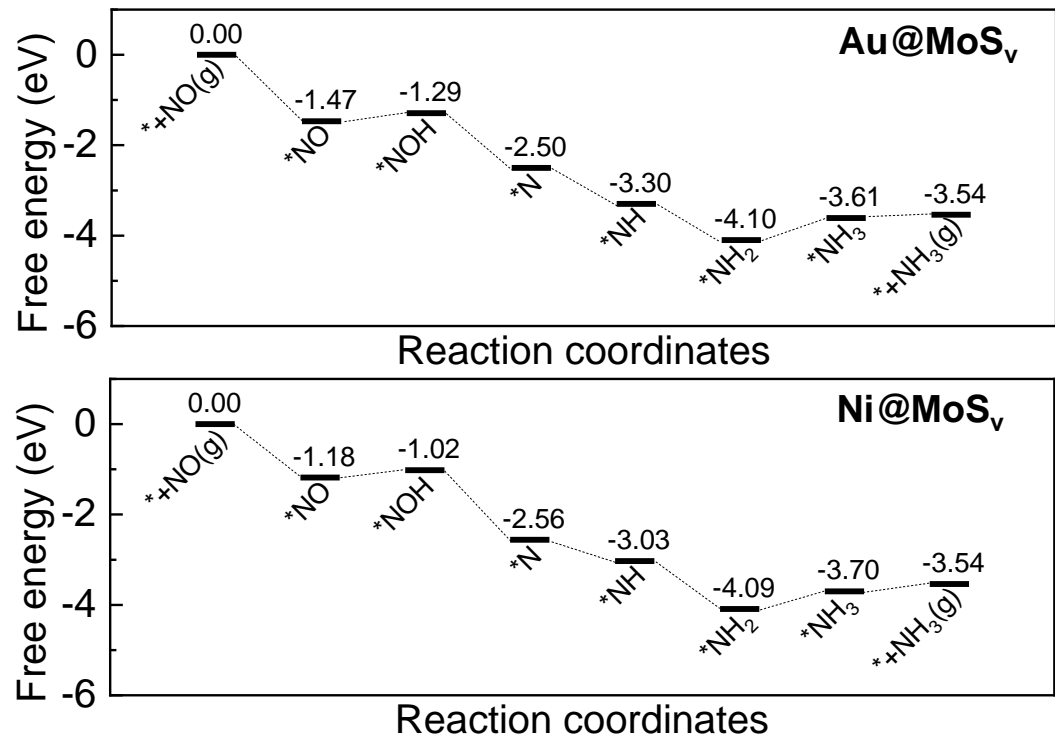
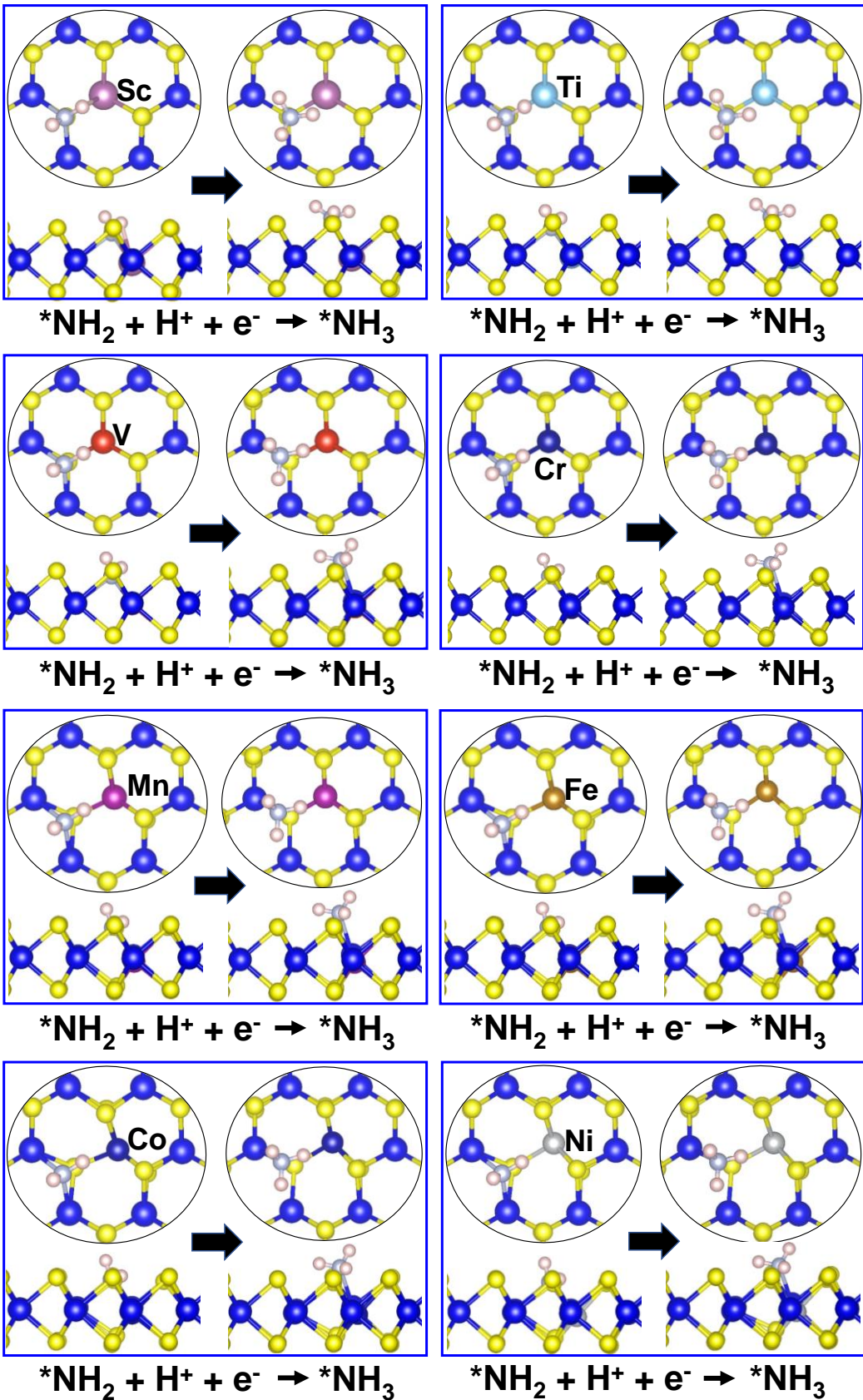
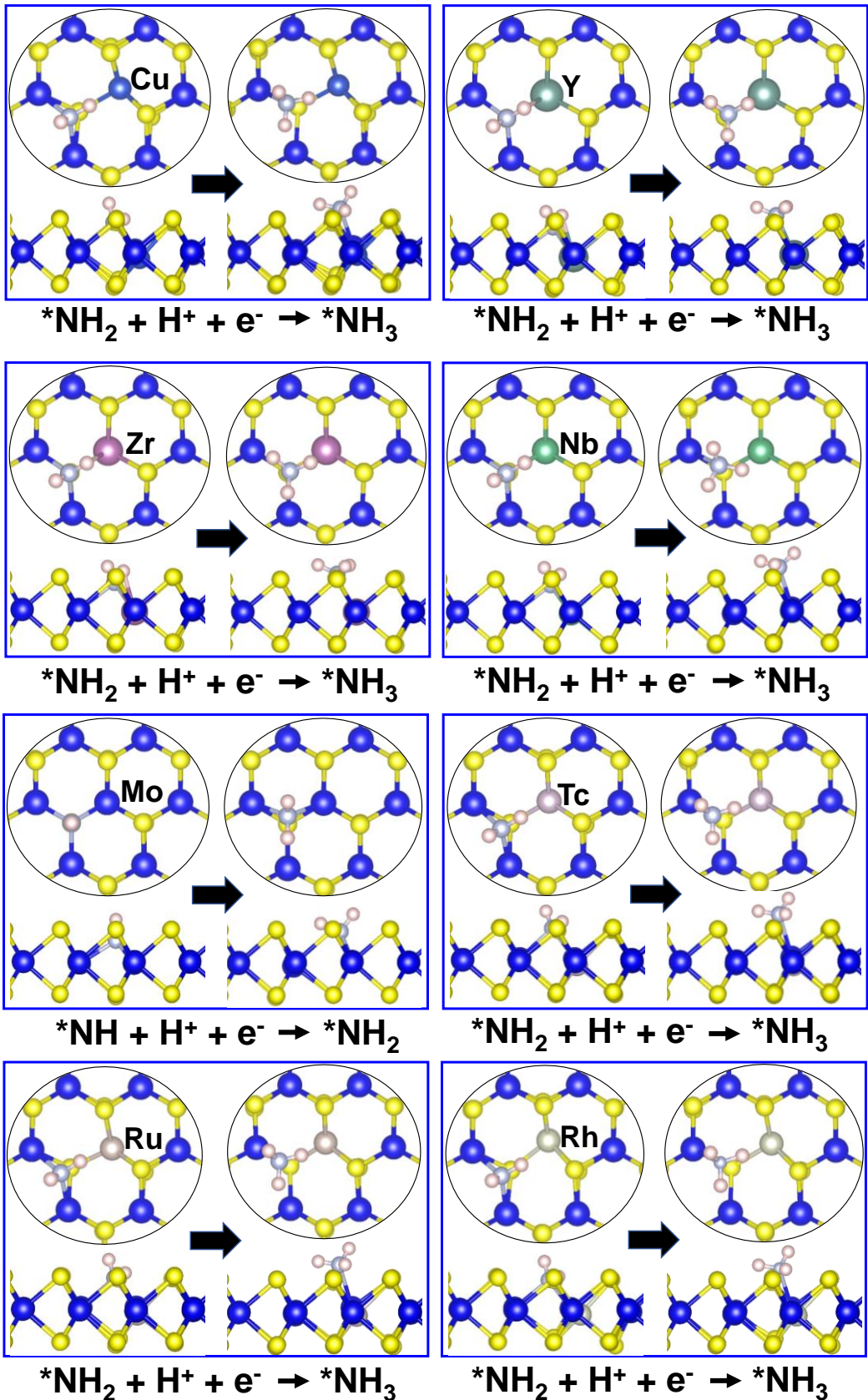
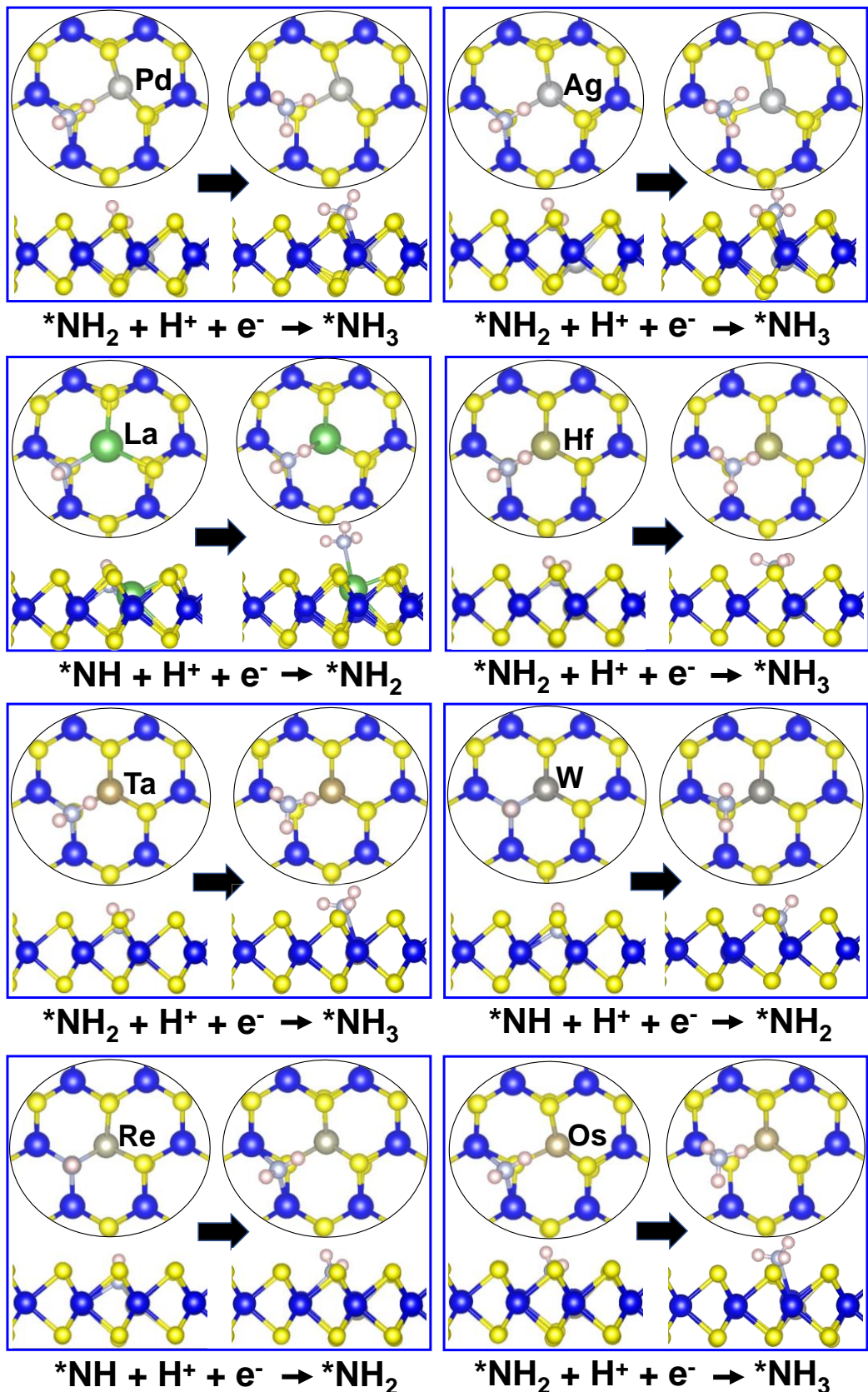


Fig. S8 Free energy diagrams for NORR on various TM@MoS_v.







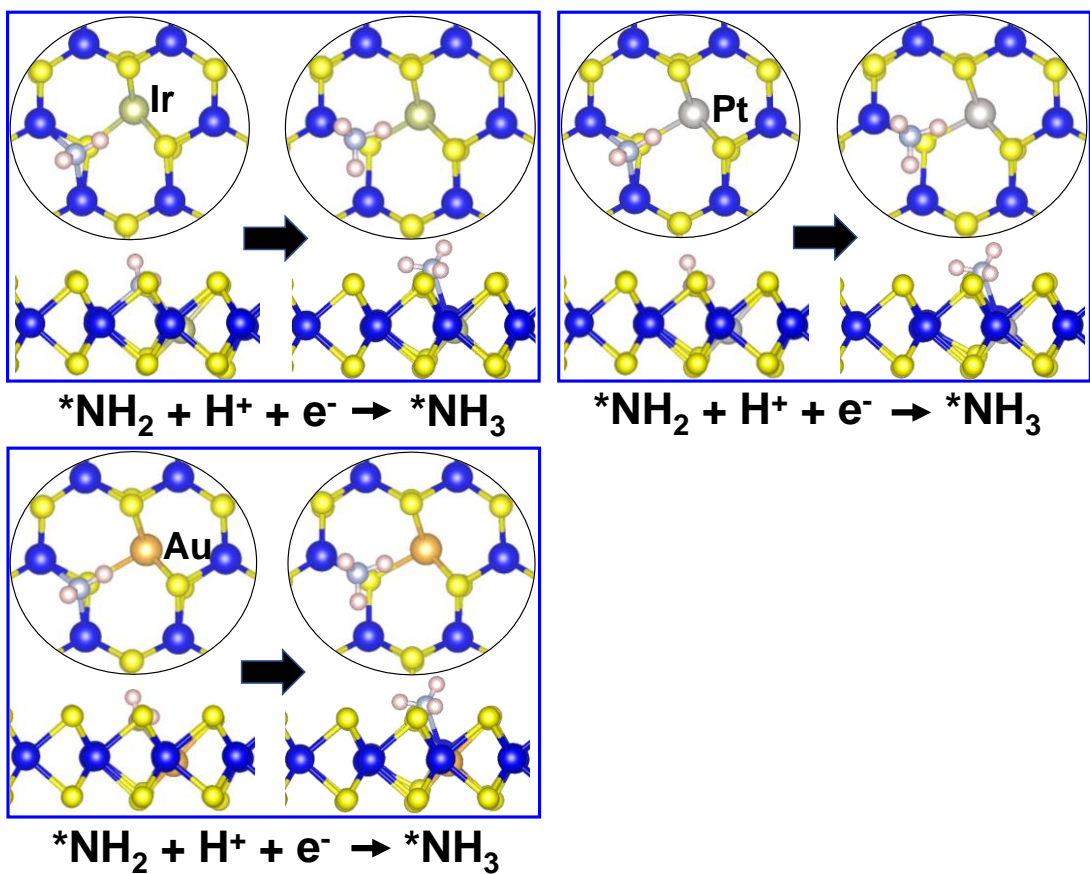


Fig. S9 Potential-determining steps for NORR on various TM@MoS_v with the local atomic configurations.

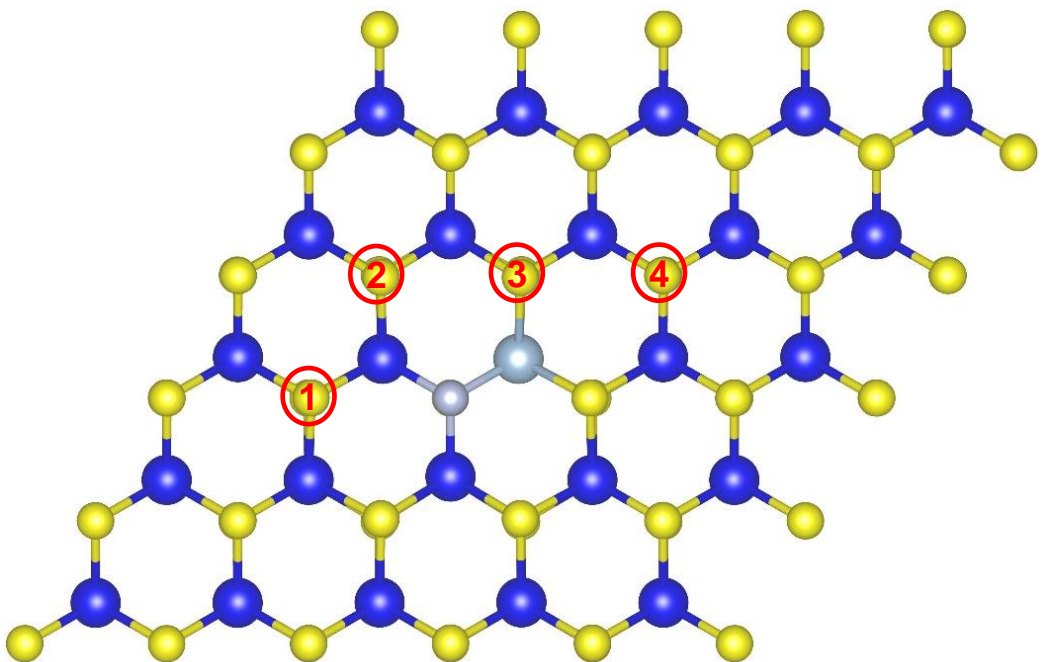
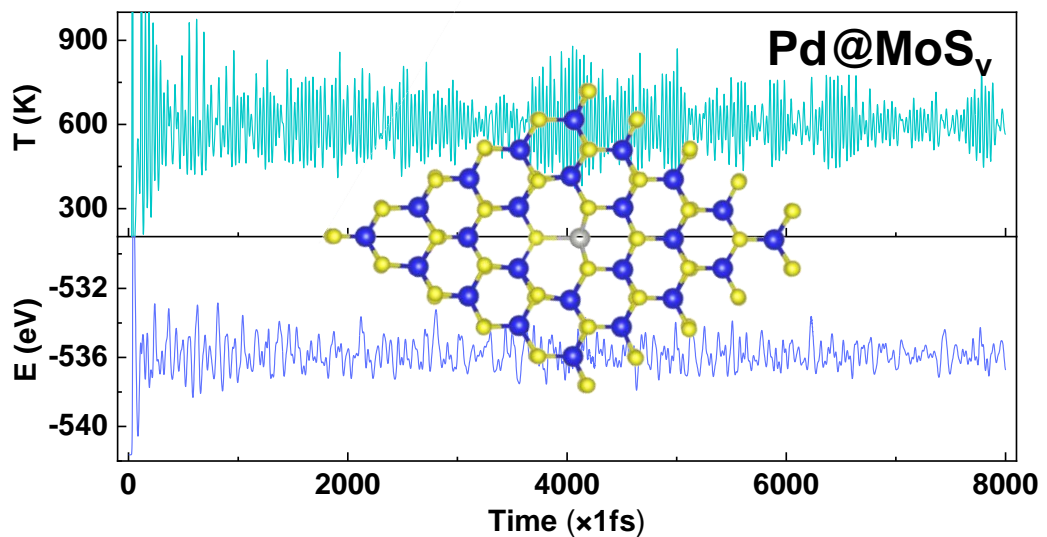
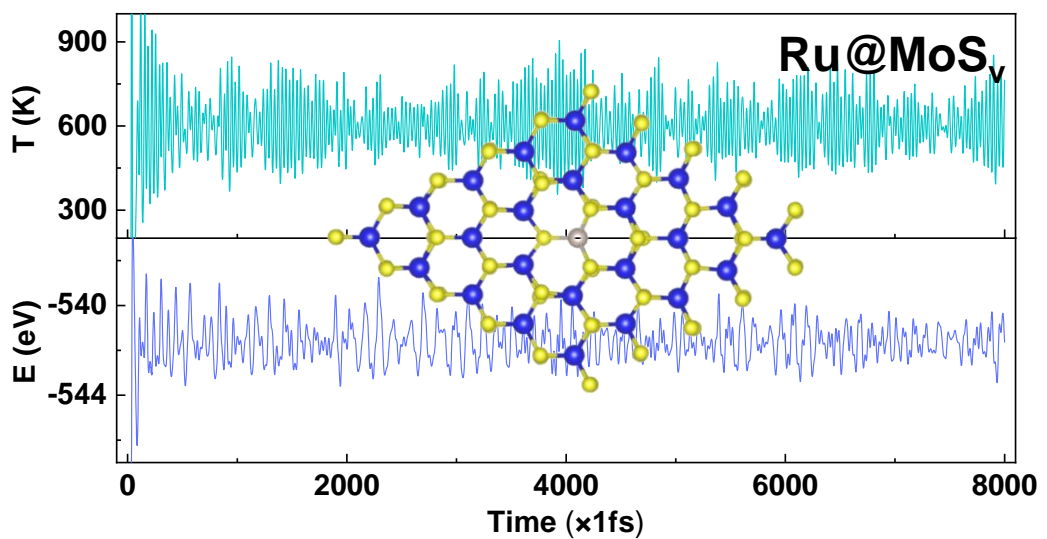
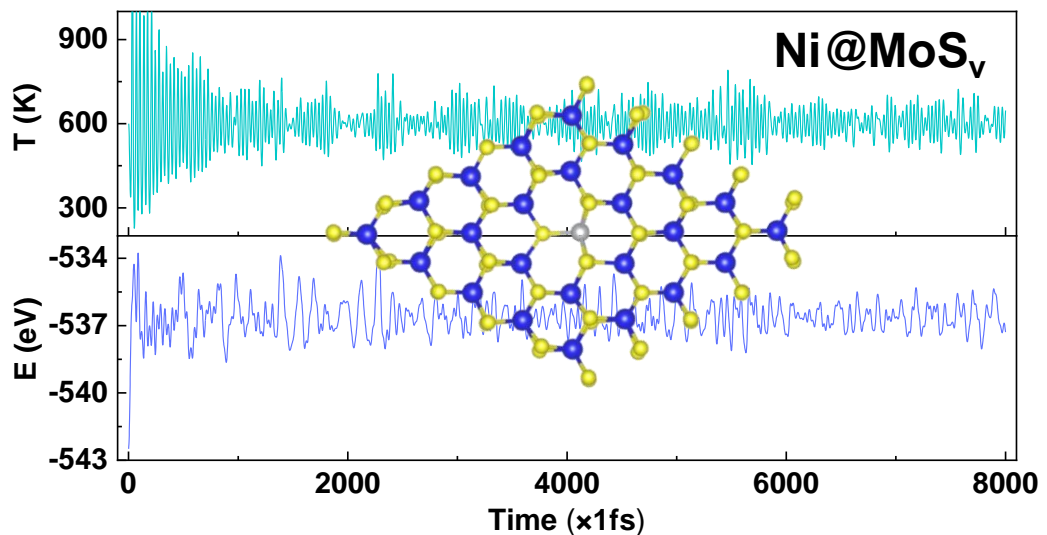


Fig. S10 The four considered N adsorption sites near the S vacancy.



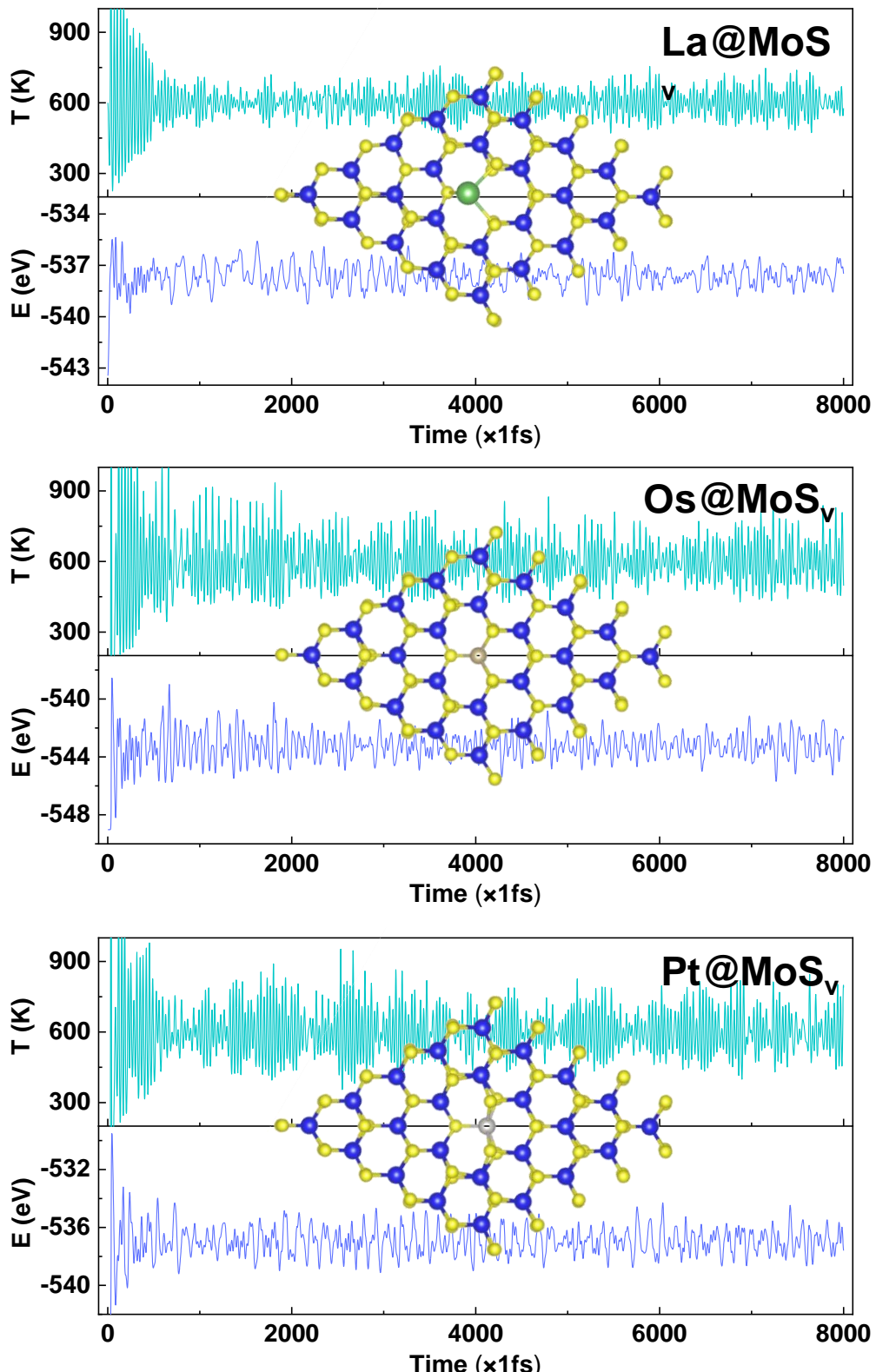


Fig. S11 The temperature and total energy variation against time through the AIMD simulation for Ni@MoS_v, Ru@MoS_v, Pd@MoS_v, La@MoS_v, Os@MoS_v and Pt@MoS_v. The simulation was performed under 600 K for 8 ps with a time-step of 1 fs. The top view of the final configuration after the simulation are shown as insets.

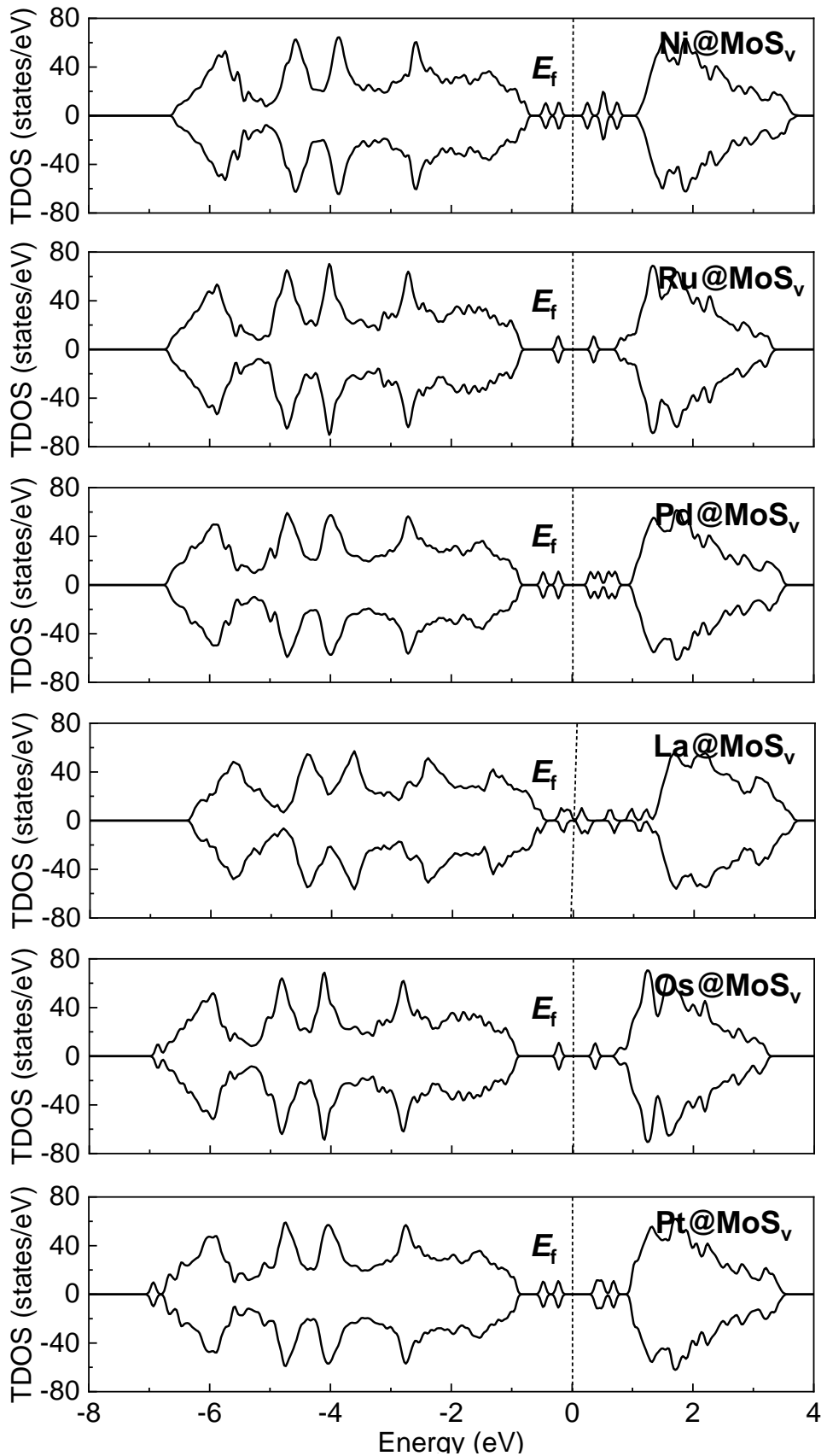


Fig. S12 Total densities of states (TDOS) for Ni@MoS_v, Ru@MoS_v, Pd@MoS_v, La@MoS_v, Os@MoS_v and Pt@MoS_v. The E_f is set to be 0 eV.

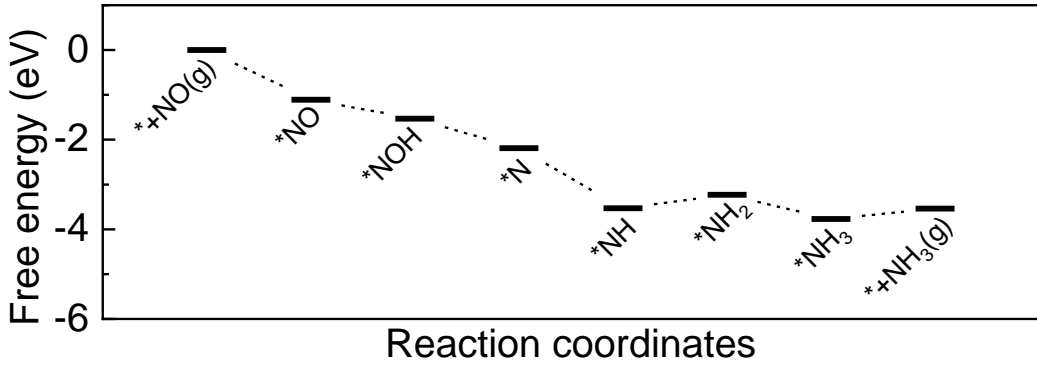


Fig. S13 Free energy diagrams of NORR on La@MoS_v with the solvation correction.

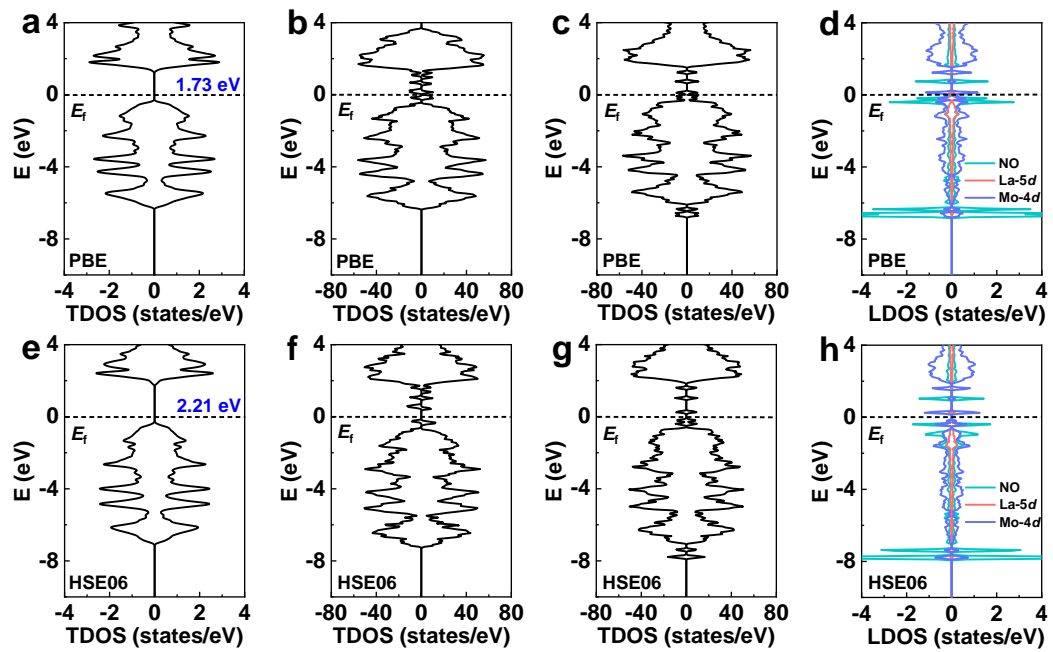


Fig. S14 (a) and (e) are for the total densities of states (TDOS) of the MoS₂ monolayer unit cell. (b) and (f) are for the TDOS of La@MoS_v. (c) and (g) are for the TDOS of NO-adsorbed La@MoS_v. (d) and (h) are the local densities of states (LDOS) of the *NO, and its bonded La (5d states) and Mo (4d states) of the NO-adsorbed La@MoS_v. For (a-d), the PBE functional has been used, while for (e-h) the HSE06 functional has been used.

References:

1. Z. Li, Z. Ma, J. Liang, Y. Ren, T. Li, S. Xu, Q. Liu, N. Li, B. Tang, Y. Liu, S. Gao, A. A. Alshehri, D. Ma, Y. Luo, Q. Wu and X. Sun, *Mater. Today Phys.*, 2022, **22**, 100586.
2. H. Niu, Z. Zhang, X. Wang, X. Wan, C. Kuai and Y. Guo, *small*, 2021, **17**, 2102396.
3. J. L. L. Zhang, Y. Wang, T. Mou, Y. Lin, L. Yue, T. Li, Q. Liu, Y. Luo, N. Li, B. Tang, Y. Liu, S. Gao, A. A. Alshehri, X. Guo, D. Ma, and X. Sun., *Angew. Chem. Int. Ed.*, 2021, **60**, 25263–25268.
4. P. Liu, J. Liang, J. Wang, L. Zhang, J. Li, L. Yue, Y. Ren, T. Li, Y. Luo, N. Li, B. Tang, Q. Liu, A. M. Asiri, Q. Kong and X. Sun, *Chem. Commun.*, 2021, **57**, 13562–13565.
5. Y. Lin, J. Liang, H. Li, L. Zhang, T. Mou, T. Li, L. Yue, Y. Ji, Q. Liu, Y. Luo, N. Li, B. Tang, Q. Wu, M. S. Hamdy, D. Ma and X. Sun, *Mater. Today Phys.*, 2022, **22**, 100611.
6. J. Liang, Q. Zhou, T. Mou, H. Chen, L. Yue, Y. Luo, Q. Liu, M. S. Hamdy, A. A. Alshehri, F. Gong and X. Sun, *Nano Res.*, 2022, **15**, 4008–4013.
7. Y. Li, C. Cheng, S. Han, Y. Huang, X. Du, B. Zhang and Y. Yu, *ACS Energy Lett.*, 2022, **7**, 1187–1194.
8. Y. Zang, Q. Wu, S. Wang, B. Huang, Y. Dai and Y. Ma, *J. Phys. Chem. Lett.*, 2022, **13**, 527–535.
9. Z. Wang, J. Zhao, J. Wang, C. R. Cabrera and Z. Chen, *J. Mater. Chem. A*, 2018, **6**, 7547–7556.
10. Q. Wu, W. Wei, X. Lv, Y. Wang, B. Huang and Y. Dai, *J. Phys. Chem. C*, 2019, **123**, 31043–31049.
11. P.-F. Sun, W.-L. Wang, X. Zhao and J.-S. Dang, *Phys. Chem. Chem. Phys.*, 2020, **22**, 22627–22634.
12. Y. Xiao and C. Shen, *Small*, 2021, **17**, 2100776.
13. I. Katsounaros, M. C. Figueiredo, X. Chen, F. Calle-Vallejo and M. T. M. Koper, *ACS Catal.*, 2017, **7**, 4660–4667.
14. T. Mou, J. Liang, Z. Ma, L. Zhang, Y. Lin, T. Li, Q. Liu, Y. Luo, Y. Liu, S. Gao, H. Zhao, A. M. Asiri, D. Ma and X. Sun, *J. Mater. Chem. A*, 2021, **9**, 24268–24275.